The influence of Cu on metastable $NiSn_4$ in Sn-3.5Ag-xCu /ENIG joints

S.A. Belyakov*, C.M. Gourlay
Department of Materials, Imperial College, London SW7 2AZ, United Kingdom

Corresponding author:

Sergey A. Belyakov

Department of Materials
Imperial College
London
SW7 2AZ
United Kingdom
+44 20 7594 6746
s.belyakov@imperial.ac.uk

e-mail addresses of all authors:
C. Gourlay: c.gourlay@imperial.ac.uk
S.Belyakov: s.belyakov@imperial.ac.uk

ABSTRACT

We explore the effect of dilute Cu additions on the suppression of metastable βSn-$NiSn_4$ eutectic growth in solder joints between Sn-3.5Ag-xCu solders and Ni-based substrates. In Sn-3.5Ag/electroless nickel immersion gold (ENIG) or Sn-3.5Ag/Ni solder joints, it is shown that the eutectic mixture contains βSn, Ag_3Sn and metastable $NiSn_4$. It is found that additions of only 0.005wt%Cu to Sn-3.5Ag-xCu/ENIG or Sn-3.5Ag-xCu/Ni joints promote the formation of stable βSn-Ni_3Sn_4 eutectic and that both Ni_3Sn_4 and $NiSn_4$ exist in the eutectic at this Cu level. It is further shown that for the full prevention of metastable $NiSn_4$ during eutectic solidification of the solder joint, more considerable Cu additions of at least 0.3wt%Cu are required.

Keywords: Microstructure, Pb-free soldering, Metastable, $NiSn_4$, Intermetallics, Solidification

1 INTRODUCTION

Sn-Ag solders are a popular choice for consumer and power electronics [1] and the Sn-3.5Ag composition is frequently used on Ni-containing surface finishes, such as electroless nickel immersion gold (ENIG) and electroless nickel, electroless palladium immersion gold (ENEPIG), and on Ni-based UBMs (underbump metallizations). Solder reactions in the Sn/Ni and Sn-Ag/Ni systems and subsequent microstructure evolution have been widely studied [2-15] and most researchers reported Ni_3Sn_4 as the major interfacial reaction product in such systems, similar to that shown in Figure 1A. At the same time, it is known that non-equilibrium Sn-Ni intermetallics can form in Sn-Ni couples after soldering or during storage at elevated temperatures. In most cases non-equilibrium Sn-Ni compounds such as Ni_3Sn_8 [16], $NiSn_3$ [17-21] and $NiSn_4$ [22-24] were found after solid state ageing or thermal cycling [16-19, 21-24] or after heat treatments combined with electric current passage through the joint [19, 22]. Figure 2A is an example of non-equilibrium $NiSn_4$ formed at the interface during solid state ageing of Sn-Ni electroplated couples. The rapid growth of metastable Ni_xSn_y intermetallics during ageing, similar to Figure 2A, has been demonstrated to cause reliability concerns affecting solderability of Sn-plated component terminations [16, 18]

Most past investigations of the Sn/Ni solder system have focused on interfacial reactions, and only a very small body of research has been devoted to intermetallic (IMC) phase formation in the bulk of such solder joints. Recently, we have discovered that a metastable $NiSn_4$ phase can form during solidification of Sn-Ni alloys [25] as well as during solidification of Sn-rich solders on Ni-containing substrates [26, 27]. In each case, $NiSn_4$ forms in a eutectic reaction. Figure 2 summarises typical examples of metastable $NiSn_4$ that grows in the solder bulk by a eutectic reaction when commercial purity (CP) Sn is reflowed on pure Ni, ENIG or Fe-42Ni (Alloy 42) substrates. These three substrates yield different volume fractions of $NiSn_4$ in the bulk. As $NiSn_4$ has a substantial solubility for gold [27], all Au dissolved from the 60nm Au capping layer on ENIG goes into $NiSn_4$, which results in higher volume fractions of $NiSn_4$ eutectic on ENIG surface finishes than on pure Ni or Fe-42Ni (Figure 2B). In contrast, when soldered to Alloy42, the $FeSn_2$ interfacial intermetallic layer serves as an efficient diffusion barrier limiting the amount of Ni that dissolves into the liquid solder during reflow [28, 29]. As result, this type of solder joints has less $NiSn_4$ in the bulk solder than on Ni or ENIG substrates(Figure 2D). We have also found that trace Fe additions promote metastable $NiSn_4$ formation due to epitaxial nucleation of $NiSn_4$ on $FeSn_2$ particles [30].

We have recently demonstrated [27] that industrially important Sn-3.5Ag/ENIG or Sn-3.5Ag/Ni joints also solidify to contain metastable Sn-$NiSn_4$ eutectic (Figure 2A-C, E). Surprisingly, despite the fact that Sn-Ag solders have been used on Ni-containing substrates for decades, this phenomenon was missed in past research. $NiSn_4$ is a metastable phase and can transform into equilibrium Ni_3Sn_4 and βSn whilst the solder joint is in service at elevated temperatures [25, 27]. In automotive and power electronics, operation temperatures are relatively high (175-200°C) and microstructural stability and reliability of solder joints becomes of great interest [1]. In addition to its metastable nature, $NiSn_4$ is a brittle intermetallic compound (similar to $AuSn_4$) and can compromise solder joint mechanical properties

[27]. Controlling the formation of βSn-$NiSn_4$ eutectic might help to improve microstructural stability of solder joints subjected to high operational temperatures and also to eliminate the possibility of solder joint embrittlement by coarsened $NiSn_4$ crystals.

As a next step, we are seeking ways to suppress βSn-$NiSn_4$ eutectic growth in solder joints between Sn-Ag and Ni-based substrates. This paper explores the role of trace Cu additions because, in our solidification studies of Sn-rich Sn-Ni alloys [25], we noticed that Cu impurities as little as ~0.002wt% can affect competition between the metastable Sn-$NiSn_4$ and stable Sn-Ni_3Sn_4 eutectics. This amount of Cu resulted in the formation of traces of Sn-$(Ni,Cu)_3Sn_4$ eutectic containing up to 11at%Cu [25]. As an example, Figure 3 demonstrates $(Ni,Cu)_3Sn_4$ eutectic that was sometimes found growing from primary Ni_3Sn_4 crystals (that contain negligible Cu) in a Sn-0.37wt%Ni alloy. Additionally, during the soldering of pure Sn to ENIG-coated copper we found that, if the ENIG layer is cracked, the dissolution of Cu through the cracks during soldering promotes the formation of stable βSn-Ni_3Sn_4 eutectic [26]. These two observations suggest that higher Cu additions may promote stable βSn-Ni_3Sn_4 eutectic formation. To explore this in more detail, in the present study we use a range of Cu additions (spanning from 0.005 to 0.5wt%Cu) added to Sn-3.5Ag solder reflowed on Ni and ENIG substrates.

The aims of the present investigation were (i) to understand the role of Cu in the formation of stable Sn-Ni_3Sn_4 eutectic in industrially-relevant solder/substrate combinations and (ii) to find the critical Cu level at which formation of metastable $NiSn_4$ is eliminated in Sn-3.5Ag-xCu joints on Ni and ENIG.

2 EXPERIMENTAL PROCEDURES

Sn-3.5Ag-xCu (x=0.005-0.5wt% Cu) solders and Sn-xNi (x=0.03-0.4wt% Ni) alloys were produced by mixing the required amount of a 99.99%Ag, Sn-10wt%Cu or Sn-10wt%Ni master alloys with 200g of 99.9%Sn in a graphite crucible and heating in a resistance furnace to 450°C. After 1-h holding, the melt was drawn into 4mm quartz tubes under vacuum.

Ni and ENIG-plated Cu substrates were made from 500µm sheets of 99.9Ni or 99.9Cu. ENIG plating produced a ~5µm Ni-P layer containing 16at%P and a 60nm Au layer. Prepared substrates were cut into 10 x 10mm coupons. Some of the solder rods were rolled to 100µm foils and cut into 1 x 1cm preforms and placed on the coupons with mildly activated rosin based flux RM5. Soldering was conducted in a Tornado LFR400 reflow furnace with a heating rate of 1 K/s, time above Sn-Ag eutectic temperature of ~80 s, peak temperature of 250°C and a cooling rate of 3 K/s.

Differential scanning calorimetry (DSC) experiments were conducted using a Mettler-Toledo DSC. 250(±10) mg samples containing 0.03, 0.2 and 0.4wt% Ni were cut from 4mm rods and placed into alumina pans. The specimens were heated at 10K/min up to 350°C and cooled to room temperature at a variety of rates: 1K/min, 20K/min and 50K/min.

For metallographic investigations, all samples were mounted in Struers VersoCit acrylic cold mounting resin and wet ground to 2400 grit silicon carbide paper followed by polishing with colloidal silica. For better visualization of the three-dimensional morphology of eutectic phases, the βSn matrix was selectively etched with a solution of 5% NaOH and 3.5% orthonitrophenol in distilled H_2O. Samples were immersed in the etchant at 60°C for about 30 seconds. To obtain $NiSn_4$ eutectic intermetallic particles for transmission electron microscopy (TEM) analysis, Sn-0.2Ni samples solidified at 20K/min in the DSC were selectively etched and $NiSn_4$ eutectic was collected. Selected area diffraction patterns (SADP) were obtained using Japan Electron Optics Laboratory JEOL 2000FX TEM with an acceleration voltage of 200kV. Specimens were further investigated using a Zeiss AURIGA Field Emission Gun scanning electron microscope (FEG-SEM) equipped with an Oxford Instruments INCA x-sight energy dispersive X-ray (EDX) detector and Oxford Instruments Nordlys S electron backscattered diffraction (EBSD) detector.

3 RESULTS AND DISCUSSION

3.1 Identification of the $NiSn_4$ phase

First, we identify the metastable Ni_xSn_y phase that forms during eutectic solidification of Sn-rich Sn-Ni alloys using a combination of SEM-EDX, EBSD and TEM techniques. Figure 4A depicts a typical cross-section of a Sn-0.2Ni sample cooled at 20K/min in a DSC. The majority of the microstructure is eutectic with some primary intermetallic near the surface. Higher magnification imaging reveals a sheet-like eutectic (Figure 4B). Even though DSC experiments provided multidirectional heat flow during solidification, many eutectic sheets are aligned along distinct directions, which is consistent with previous findings in [25]. EDX measurements on the Ni_xSn_y intermetallic in the eutectic resulted in a composition close to $NiSn_4$ as summarised in Table 1.

For the EBSD study, more than 20 EBSD patterns from the eutectic particles were collected and analyzed. An example of an EBSD pattern is shown in Figure 4C. The obtained Kikuchi patterns were compared with all reported equilibrium and metastable Ni_xSn_y phases [31-33], including the oC20-$NiSn_4$ phase proposed by Boettinger et al. [24] and the tP10-$NiSn_4$ phase proposed by Watanabe et al. [34] and modelled by Ghosh [35]. Furthermore, since $NiSn_4$ is not an established phase, the Kikuchi patterns of prototypes β$IrSn_4$ [36] and $PtPb_4$ [37] were also analysed for comparison. The result of the EBSP analysis is summarized in Table 2, where all 20 EBSD patterns were used to deduce the mean angular deviation (MAD). MAD is a measure of how well positions of the bands in the simulated EBSP match those in the actual EBSP. 8 diffraction bands of the highest intensity were used whilst measuring MAD. With this approach, the EBSD patterns could only be successfully indexed as the *oC*20-XSn_4 structure of $PtSn_4$, $PdSn_4$ and $AuSn_4$ (Table 2 and Figure 4D) and were not indexable as any other known solution, similar to the work of Boettinger et al. [24]. The average MAD during fitting of the collected EBSPs to the oC20-$NiSn_4$ crystal structure was 0.42° (Table 2).

Figure 4E demonstrates a typical TEM selected area electron diffraction pattern (SAEDP) from a $NiSn_4$ eutectic sheet viewed along the [001] zone axis. The SAEDP is indexed to the oC20-$PtSn_4$ structure and the a and b lattice parameters were measured to be a = 6.25Å and b = 6.29Å based on analysis of 6 SAEDPs. Note that EBSD patterns were successfully indexed assuming structures with somewhat higher a and b lattice parameters (Table 2) than those measured from TEM-SAEDPs. This is because EBSD indexing is not highly sensitive to absolute lattice parameters. From SEM-EDX, EBSD and TEM, it is confirmed that $NiSn_4$ is isomorphous to oC20-$PtSn_4$, $PdSn_4$ and $AuSn_4$ crystals. Note that, in the commercial purity Sn-0.2Ni sample cooled at 0.33 K/s in Figure 3, all of the eutectic is metastable Sn-$NiSn_4$ eutectic and not stable Sn-Ni_3Sn_4 eutectic, which is similar to [25, 30, 38]. It is also interesting to note that recent studies have reported metastable $CoSn_4$ to have structure also isomorphous to oC20-$PtSn_4$, $PdSn_4$ and $AuSn_4$ [39]

3.2. $NiSn_4$ in joints between Sn-3.5Ag-xCu and ENIG or Ni.

The soldering of Sn-3.5Ag to pure Ni produces a Sn-Ag_3Sn-$NiSn_4$ eutectic in the bulk solder rather than the Sn-Ag_3Sn-Ni_3Sn_4 that would be expected from the equilibrium phase diagram, as shown in [27]. In that study, EBSD analysis confirmed that the $NiSn_4$ phase is of oC20-$PtSn_4$ type, similar to $NiSn_4$ in binary Sn-Ni alloys in Figure 4.

The soldering of Sn-3.5Ag to ENIG produces similar results but the dissolved Au capping layer segregates to the $NiSn_4$ phase and the eutectic is Sn-Ag_3Sn-$(Ni,Au)Sn_4$. Figure 5A,C illustrates a representative microstructure of a Sn-3.5Ag/ENIG solder joint. As can be seen from the cross-section, the bulk solder microstructure contains a large volume fraction of βSn dendrites surrounded by eutectic. There are two types of eutectic morphologies that can be differentiated in the optical micrograph in Figure 5A: (i) a dark grey dot-like and (ii) a light grey plate-like eutectic. After selective etching of βSn it can be seen that the dot-like eutectic in 2D appears as a rod-like phase in 3D and the plate-like eutectic in 2D is large but very thin sheets in 3D. SEM-EDX coupled with EBSD analysis confirmed the two intermetallic phases in the eutectic mixture: the rod-like eutectic corresponded to

Ag_3Sn and the sheet-like eutectic corresponded to $(Ni,Au)Sn_4$ (Table 3). Comparing Table 1 and Table 3, note that the $NiSn_4$ in Sn-0.2Ni alloy and the $(Ni,Au)Sn_4$ in Sn-3.5Ag/ENIG joints have the same Sn content of ~81-82at% Sn, and that Au atoms substitute for Ni atoms in $(Ni,Au)Sn_4$. Also note that $(Ni,Au)Sn_4$ contains ~13at%Ni and ~6at%Au which is higher than the reported maximum solubility of Ni in $AuSn_4$ [40] and, therefore, it is likely that $(Ni,Au)Sn_4$ is metastable $NiSn_4$ with dissolved Au. The decomposition of metastable $(Ni,Au)Sn_4$ during aging of Sn-3.5Ag/ENIG joints is presented in [27].

Figure 5B,D is a representative microstructure of a Sn-3.5Ag-0.005Cu/ENIG joint that can be compared with the Sn-3.5Ag/ENIG joint in Figure 5A,C. The major difference was the presence of a darker phase in the eutectic in optical micrographs (Figure 5B). SEM-EDX analysis confirmed the presence of a third intermetallic phase in the eutectic mixture: Ni_3Sn_4 with ~4at%Cu, as summarised in Table 3. The interfacial Ni_3Sn_4 IMC layer was not found to contain Cu in amounts more than 1at% (which is just above the resolution limit of the EDX technique with the settings used). Additionally, the eutectic $NiSn_4$ was found to dissolve negligible Cu (Table 3). The key result in Figure 5 is that an addition of only 0.005wt%Cu (50 ppm) is sufficient to cause some stable Ni_3Sn_4 to form in the bulk solder of a Sn-3.5Ag-xCu/ENIG joint and that both $(Ni,Cu)_3Sn_4$ and $NiSn_4$ are present in the eutectic mixture at this Cu level.

Figure 6 demonstrates the results of SEM-EDX mapping of a eutectic region in Sn-3.5Ag-0.005Cu soldered to an ENIG substrate. The region in Figure 6A contains all three eutectic intermetallics: Ag_3Sn, $NiSn_4$ and $(Ni,Cu)_3Sn_4$. Cu-containing Ni_3Sn_4 eutectic appeared brighter in SE-SEM images after prolonged polishing (Figure 6) as it provided the highest surface relief. It can be seen from the EDX maps in Figure 6 that Ni_3Sn_4 readily dissolves Cu, whereas $NiSn_4$ contains no discernable Cu.

Examination of eutectic regions showed that some eutectic regions contained only $\beta Sn + Ag_3Sn$ when others contained $\beta Sn + Ag_3Sn + NiSn_4$ or $\beta Sn + Ag_3Sn + NiSn_4 + (Ni,Cu)_3Sn_4$. Based on this observation, it is probable that for this multi-component system, the solidification sequence was the following: (i) $L \rightarrow \beta Sn$ primary dendrite growth (Figure 5), followed by (ii) $L \rightarrow \beta Sn + Ag_3Sn$ eutectic growth followed by (iii) $L \rightarrow \beta Sn + Ag_3Sn + NiSn_4$ and finally by (iv) $L \rightarrow \beta Sn + Ag_3Sn + NiSn_4 + (Ni,Cu)_3Sn_4$ high-order reactions. This implies that $NiSn_4$ and $(Ni,Cu)_3Sn_4$ formed during the latest solidification stages when high-order eutectic reactions took place.

Further additions of Cu to the base Sn-3.5Ag solder caused more complicated microstructural changes. Figure 7A shows the Sn-3.5Ag-xCu solders used in this study superimposed on the Sn-Ag-Cu liquidus projection from ref. [41] and Table 4 summarizes the intermetallic phases formed in the solder bulk and at the substrate interface after soldering to ENIG. Note that we are considering a 6-component system (Sn-Ag-Ni-Cu-Au-P) after substrate dissolution and we limit our analysis to the identification of the eutectic intermetallics forming in solder joints.

Table 4 shows that, in Sn-3.5Ag/Ni and Sn-3.5Ag/ENIG joints, the eutectic intermetallics are Ag_3Sn and metastable $NiSn_4$, as mentioned previously. An example of the Ag_3Sn fibrous rods and $NiSn_4$ sheets in a Sn-3.5Ag/ENIG joint is shown in Figure 7B. At the Cu level of 0.005Cu, some equilibrium Ni_3Sn_4 started to form in the eutectic (Table 4, Figure 5B,D and Figure 6). As the amount of Cu increased, the volume fraction of Ni_3Sn_4 in the eutectic increased, with a simultaneous decrease in the volume fraction of metastable $NiSn_4$. However, $NiSn_4$ existed in the eutectic mixture at 0.15wt%Cu and a Cu level of 0.3wt%Cu was required for the metastable $NiSn_4$ phase to be fully displaced by the equilibrium Ni_3Sn_4 intermetallic in the eutectic. Table 4 shows that the amount of Cu needed to fully prevent $NiSn_4$ formation is so large that the phase equilibria are significantly altered. For example, by 0.05Cu (i.e. Sn-3.5Ag-0.05Cu/ENIG), some Cu_6Sn_5 forms in the eutectic mixture and there are four intermetallic phases in the eutectic mixture(s): Ag_3Sn, $NiSn_4$, Ni_3Sn_4 and Cu_6Sn_5 with some solubilities for Cu, Ni and Au. Thus, trace Cu additions to Sn-3.5Ag solder cannot be used to fully suppress metastable $NiSn_4$ and promote Ni_3Sn_4 in the eutectic and large Cu additions (relative to the Sn-Ag-Cu phase diagram) of ~0.3wt%Cu are required to fully prevent $NiSn_4$ from forming. That is to say that Sn-3.5Ag-0.3Cu is better considered a SAC solder than a Cu-microalloyed Sn-3.5Ag solder. Note that similar results to Table 4 were obtained on pure Ni substrates and ENIG substrates.

Further increasing the Cu content to 0.5wt%Cu results in no Ni_xSn_y intermetallics in the solder bulk nor at the interface. In this case, the eutectic mixture contains Ag_3Sn and Cu_6Sn_5, and the reaction layer is Cu_6Sn_5 with dissolved Ni and Au (Table 4). Figure 7D is a typical example of the Ag_3Sn fibrous rods and Cu_6Sn_5 sheets in the eutectic and Figure 7E is a representative region of the Cu_6Sn_5 reaction layer of a Sn-3.5Ag-0.5Cu/ENIG joint. Past work has studied the variations in Cu_6Sn_5 and Ni_3Sn_4 formation and phase fractions in the eutectic and at the interfacial layer with changing Cu content in SAC alloys [42-44]. In this work we have shown that metastable $NiSn_4$ also forms and adds further complexity as summarised in Table 4.

The competition between stable and metastable eutectic growth in the Sn-Ni system are discussed in ref [25, 30]. The present study has shown that trace Cu additions affect this competition in Sn-3.5Ag-xCu/Ni joints, although not enough to be an industrially useful method to prevent metastable $NiSn_4$ formation in Sn-3.5Ag/Ni joints (unless large Cu contents are used). The mechanism by which Cu affects the competition may be related to the significant solubility of Cu in Ni_3Sn_4 and negligible solubility in $NiSn_4$ (Table 3). For example, during metastable Sn-$NiSn_4$ eutectic growth, Cu must be rejected into the liquid at Sn-L and $NiSn_4$-L interfaces whereas, in stable Sn-Ni_3Sn_4 eutectic growth, Cu partitions to the Ni_3Sn_4 phase and Cu will not build up the in liquid ahead of the interface to the same extent. However, a fundamental directional solidification study on Sn-Ni-Cu alloys is required to explore this in detail.

4. CONCLUSIONS

A study has been performed to test whether dilute Cu additions can be used to suppress metastable βSn-$NiSn_4$ eutectic growth in solder joints between Sn-3.5Ag-xCu solders and Ni-based substrates. The following conclusions can be drawn:

- When Sn-3.5Ag is soldered to Ni, the bulk solder solidifies to contain tin dendrites and a eutectic containing Sn, Ag_3Sn and metastable $NiSn_4$. No stable Ni_3Sn_4 formed in the bulk solder in Sn-3.5Ag/Ni.
- When Sn-3.5Ag is soldered to ENIG, the bulk solder microstructure is very similar to Sn-3.5Ag/Ni except that the $NiSn_4$ phase contains ~6at% Au in $(Ni,Au)Sn_4$ and the volume fraction of $(Ni,Au)Sn_4$ is higher than in Sn-3.5Ag/Ni
- An addition of only 0.005wt%Cu to Sn-3.5Ag solder has been found to be sufficient to cause some stable Ni_3Sn_4 to form in the bulk solder of a Sn-3.5Ag-xCu/ENIG joint. At this Cu level, both Ni_3Sn_4 and $NiSn_4$ are present in the eutectic mixture of the bulk solder, and the $(Ni,Cu)_3Sn_4$ eutectic contains ~4at% Cu.
- In Sn-3.5Ag-xCu/ENIG joints containing higher Cu content, the fraction of stable $(Ni,Cu)_3Sn_4$ increases and the fraction of metastable $NiSn_4$ decreases. However, some metastable $NiSn_4$ forms in the eutectic mixture at all Cu levels from 0-0.15 wt%Cu in Sn-3.5Ag-xCu/Ni or /ENIG joints.
- Only at Cu contents of ~0.3wt% and higher was the $NiSn_4$ phase eliminated from the microstructures.

From this work, it can be seen that additions of only 50ppm Cu to Sn-3.5Ag-xCu/ENIG joints promote the formation of stable Ni_3Sn_4 in the eutectic, but a large Cu content of ~0.3wt%Cu is required to fully prevent $NiSn_4$ formation during eutectic solidification of the solder joint. A composition Sn-3.5Ag-0.3Cu is better considered a SAC solder than a Cu-microalloyed Sn-3.5Ag solder.

ACKNOWLEDGEMENTS

This research was funded by Nihon Superior Co., Ltd. and UK EPSRC grant EP/M002241/1.

REFERENCES

1. B.T Zhou, G. Muralidharan, K. Kurumadalli, C.M. Parish, S. Leslie and T.R. Bieler, *J. Electron. Mater.* 43, 57 (2014).
2. H.Y. Chen and C. Chen, *J. Electron. Mater.* 38, 338 (2009).
3. D. Gur and M. Bamberger, *Acta Mater.* 46, 4917 (19998).
4. S. Bader, W. Gust and H. Hieber, *Acta Metallurg. Et Mater.* 43, 329 (1995).
5. W. J. Tomlinson and H. G. Rhodes, *J. Mater. Sci.* 22, 1769 (1987).
6. S. K. Kang and V. Ramachandran, *Scripta Metallurg.* 14, 421 (1980).
7. J. Gorlich, D. Baither and G. Schmitz, *Acta Mater.* 58, 3187 (2010).
8. J. W. Yoon, H. S. Chun and S. B. Jung, *J. Mater. Sci.-Mater. Electron.* 18, 559 (2007).
9. Y. C. Lin, K. J. Wang and J. G. Duh, *J. Electron. Mater.* 39, 283 (2010).
10. G. Zeng, S.B. Xue, L. Zhang, L.L. Gao, W. Dai and J. D. Luo, *J. Mater. Sci.-Mater. Electron.* 21, 421 (2010).
11. Y.H. Baek, B.M. Chung, Y.S. Choi, J. Choi and J.Y. Huh, *J. Alloys Compd.* 579, 75 (2013).
12. Q. Zhou, M.L. Huang, N. Zhao and Z.J. Zhang, ICEPT-HDP 2012, 1403 (2012).
13. C.E. Ho, S.W. Lin and Y.C. Lin, *J. Alloys Compd.* 509, 7749 (2011).
14. S.P. Peng, W.H. Wu, C.E. Ho and Y.M. Huang, *J. Alloys Compd.* 493, 431 (2010).
15. J.W. Yoon, B.I. Noh and S.B. Jung, IEEE Transactions, 33, 64 (2010).
16. A.C. Harman (Proc. Tech. Program. Internepcon'78, Brighton,England, 1978), pp. 42–49.
17. P. J. Kay and C.A. Mackay, and C.A. Mackay, Trans. Inst. Met. Finish. 54, 68 (1977)
18. J. Haimovich, *Weld. J.* 68, S102 (1989).
19. C. M. Chen and S. W. Chen, *J Mater Res.* 18, 1293 (2003).
20. W. K. Choi and H. M. Lee, *J. Electron. Mater.* 28, 1251 (1999).
21. I. Vitina, I. Pelece, V. Rubene, V. Belmane, M. Lubane, A. Krumina and Z. Zarina, *J. Adhes. Sci. Technol.* 11, 835 (1997).
22. C. H. Wang, C.Y. Kuo, H.H. Chen and S.W. Chen, *Intermetallics* 19, 75 (2011).
23. L. J. Zhang, L. Wang, X.M. Xie and W. Kempe, IEEE-Inst Electrical Electronics Engineers Inc, Shanghai, Peoples R China, 2002, pp. 284-288.
24. W. J. Boettinger, M. D. Vaudin, M. E. Williams, L. A. Bendersky and W. R. Wagner, *J. Electron. Mater.* 32, 511 (2003).
25. S.A. Belyakov and C.M. Gourlay, *Intermetallics* 25, 48 (2012)
26. S.A. Belyakov and C.M. Gourlay, *J. Electron. Mater.* 41, 3331 (2012).
27. S.A. Belyakov and C.M. Gourlay, *Mater. Lett*. 148, 91 (2015).
28. C.W. Hwang, K. Suganuma, J.G. Lee and H. Mori, *J. Mater. Res.* 18, 1202 (2003).
29. Y.W. Yen, H.M. Hsiao, S.W. Lin, P.J. Huang and C.Y. Lee, *J. Electron. Mater.* 41, 144 (2012).
30. S.A. Belyakov and C.M. Gourlay, *Intermetallics*, 37, 32 (2013).
31. W. Jeitschko and B. Jaberg, *Acta Crystallogr.* 38, 598 (1982).
32. H. Fjellvag and A. Kjekshus, *Acta Chemica Scandinavica*, Series A (40), 23 (1986).
33. A.L. Lyubimtsev, A.I. Baranov, A. Fischer, L. Kloo, and A.B. Popovkin, *J. Alloys Compd.* 340, 167 (2002).
34. T. Watanabe, K. Arai, T. Hirose, and M. Chikazawa, *J. Japan Ins. Metal.* 63, 489 (1999).
35. G. Ghosh, *Metallurg. Mater. Trans.* 40A, 4 (2009).
36. E.L. Nordmark, O. Wallner and U. Haussermann, *J. Solid State Chem.* 168, 34 (2002).
37. U. Roesler and K. Schubert, *Zeitschrift fuer Metallkunde*, 42, 395 (1951).

38. S.A. Belyakov and C.M. Gourlay, *Acta Mater.* 71, 56 (2014).
39. C.H. Wang, S.E. Huang and C.W. Chiu, *J. Alloys Compd.* 619, 474 (2015).
40. H.Q. Dong, V. Vuorinen, T. Laurila, and M. Paulasto-Krockel, *Calphad-Comput. Coupl. Phase Diagram and Thermochem*. 43, 61 (2013).
41. K.W. Moon, W.J. Boettinger, U.R. Kattner, F.S. Biancaniello, and C.A. Handwerker, *J. Electron. Mater.* 29, 1122 (2000).
42. L. Snugovsky, P. Snugovsky, D.D. Perovic, and J.W. Rutter, *Mater. Sci. Technol.* 25, 1296 (2009).
43. T. Laurila, V. Vuorinen and J. K. Kivilahti, *Mater. Sci. Eng. R-Rep.* 49, 1 (2005).
44. C.E. Ho, R.Y. Tsai, Y.L. Lin and C.R. Kao, *J. Electron. Mater.* 31, 584 (2002).

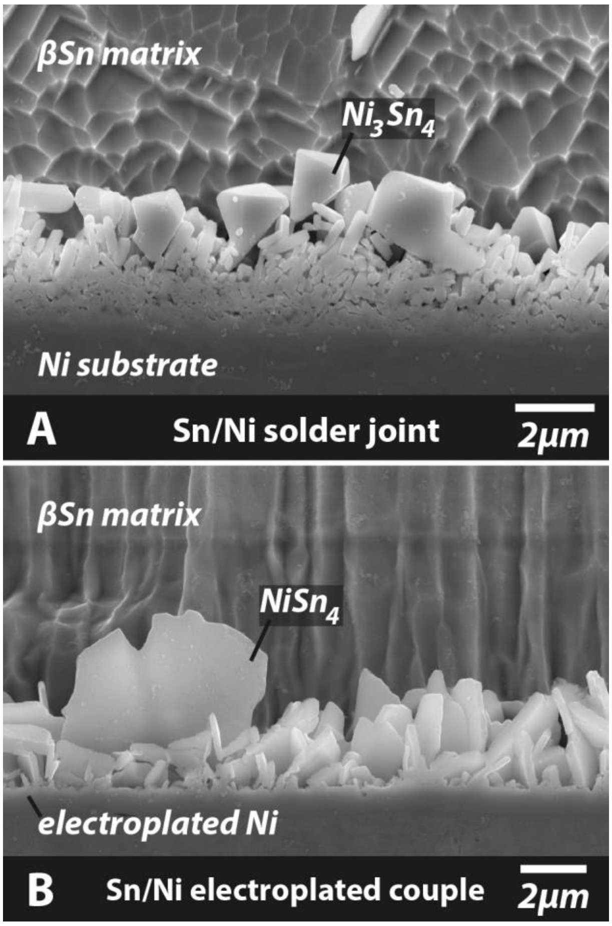

Figure 1. (A): Ni_3Sn_4 interfacial IMC layer formed during soldering of Sn to a Ni substrate; (B) $NiSn_4$ interfacial IMC layer formed at the interface of electroplated Sn on electroplated Ni after 1 month at 50°C. Note that some βSn has been selectively etched.

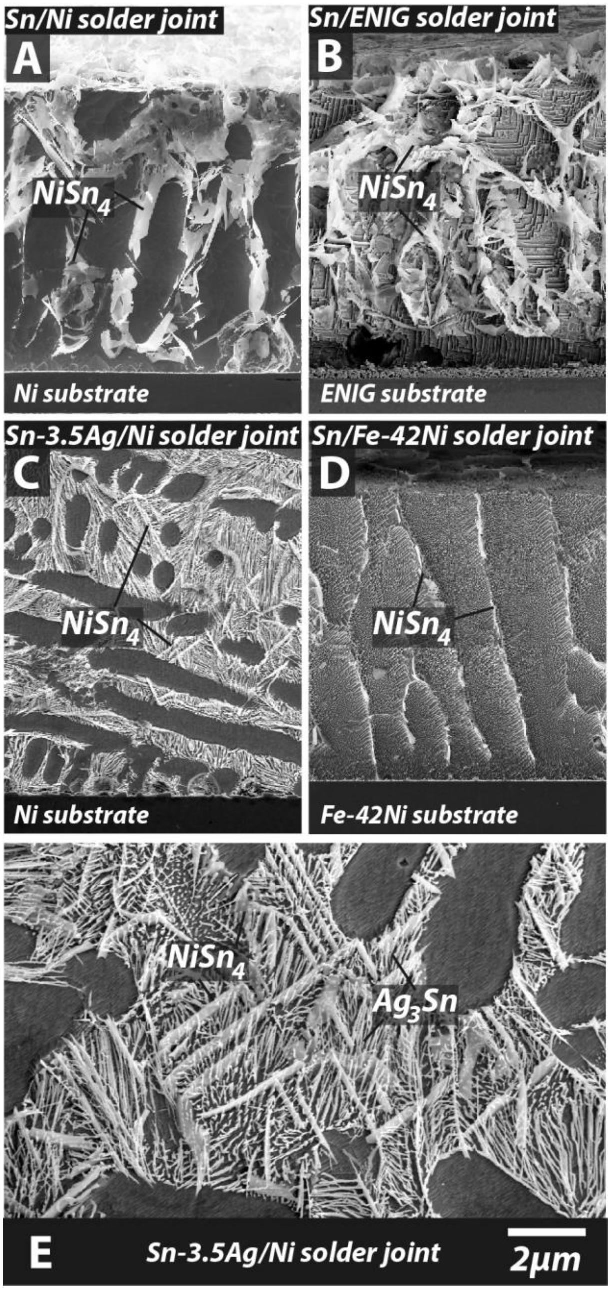

Figure 2. SEM micrographs illustrating typical $NiSn_4$ eutectic phase formed in (A) Sn/Ni solder joint; (B): Sn/ENIG solder joint; (C) and (E): Sn-3.5Ag/Ni solder joint and (D): Sn/Fe-42Ni solder joint. Note that some βSn has been selectively etched.

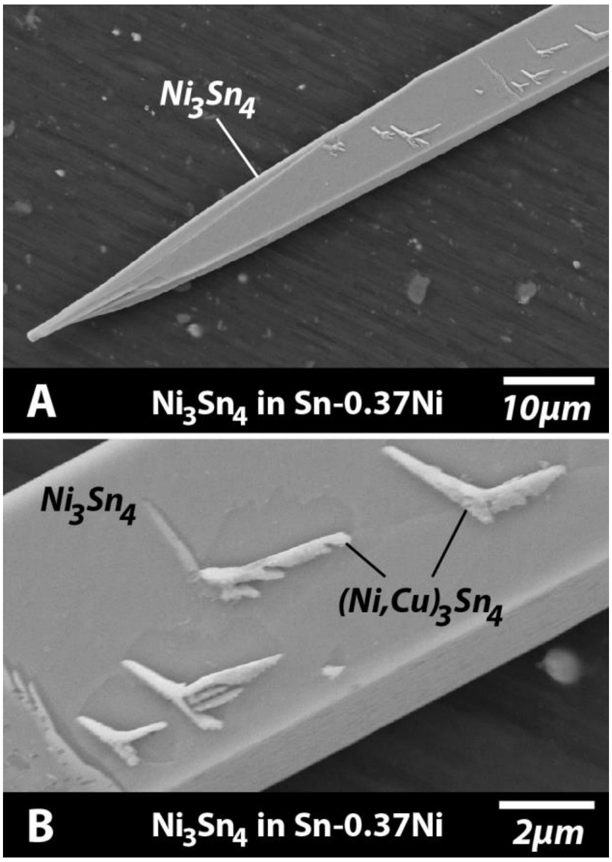

Figure 3. Primary Ni_3Sn_4 crystal formed in CP Sn-0.37Ni and traces of Ni_3Sn_4 eutectic phase growing on its facets.

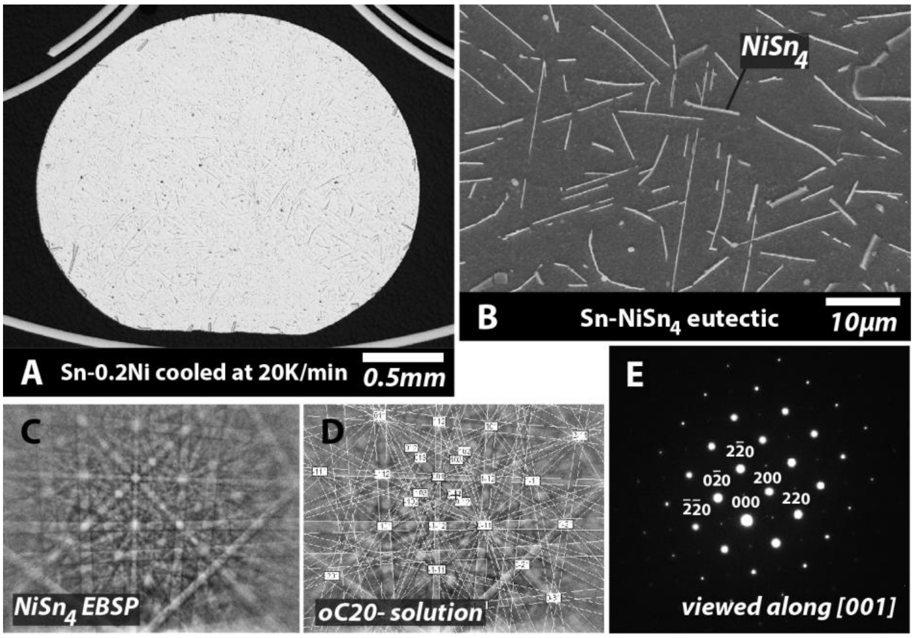

Figure 4. (A): optical micrograph of Sn-0.2Ni sample solidified at 20K/min; (B): SEM micrograph of the eutectic region in (A) after selective etching of βSn matrix; (C): representative EBSP from the eutectic in (A) and (D): indexing the EBSP as cC20-NiSn$_4$ phase; (E): representative TEM SADP collected from the NiSn$_4$ eutectic.

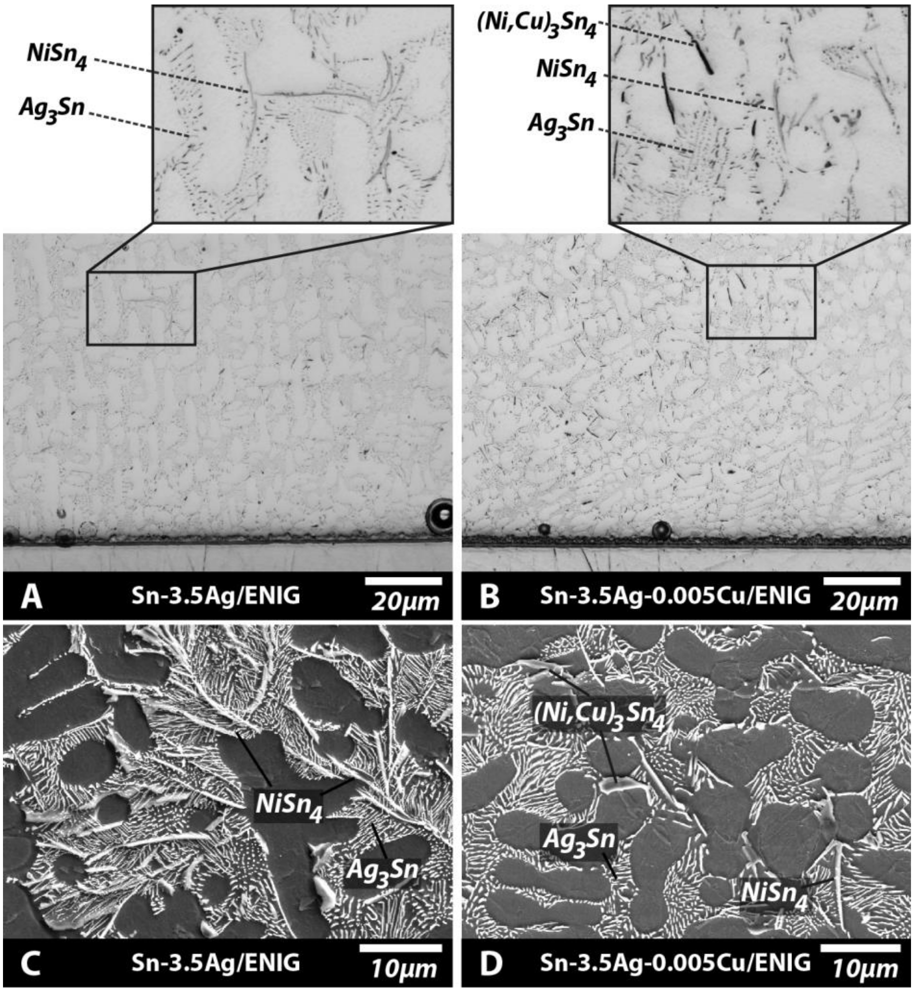

Figure 5. Optical micrographs of (A): Sn-3.5Ag/ENIG and (B): Sn-3.5Ag-0.005Cu/ENIG solder joints; SEM images after selective etching of βSn matrix of (C): Sn-3.5Ag/ENIG and (D): Sn-3.5Ag-0.005Cu/ENIG solder joints.

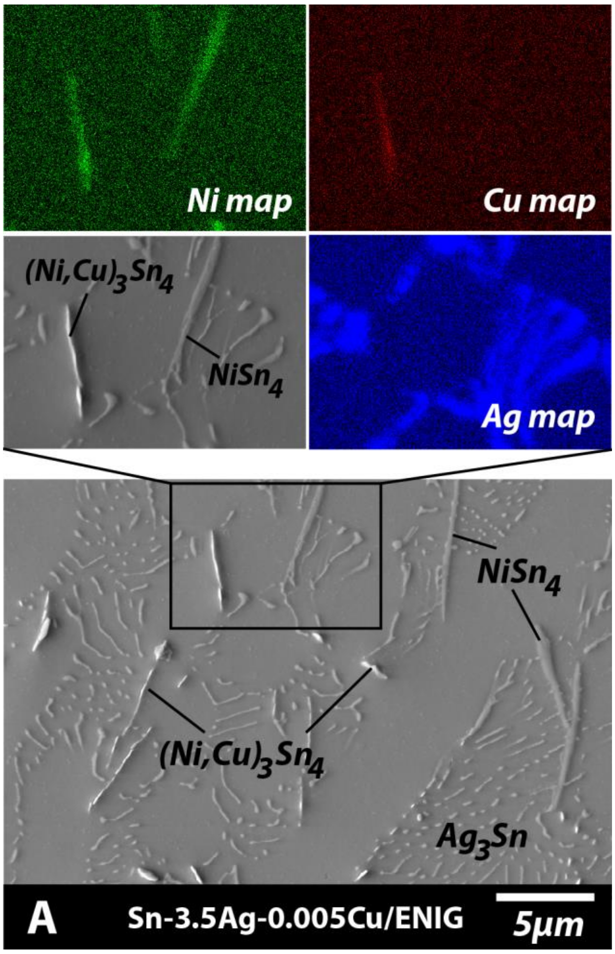

Figure 6. SEM-EDX mapping of a typical microstructure formed in Sn-3.5Ag-0.005Cu/ENIG solder joint.

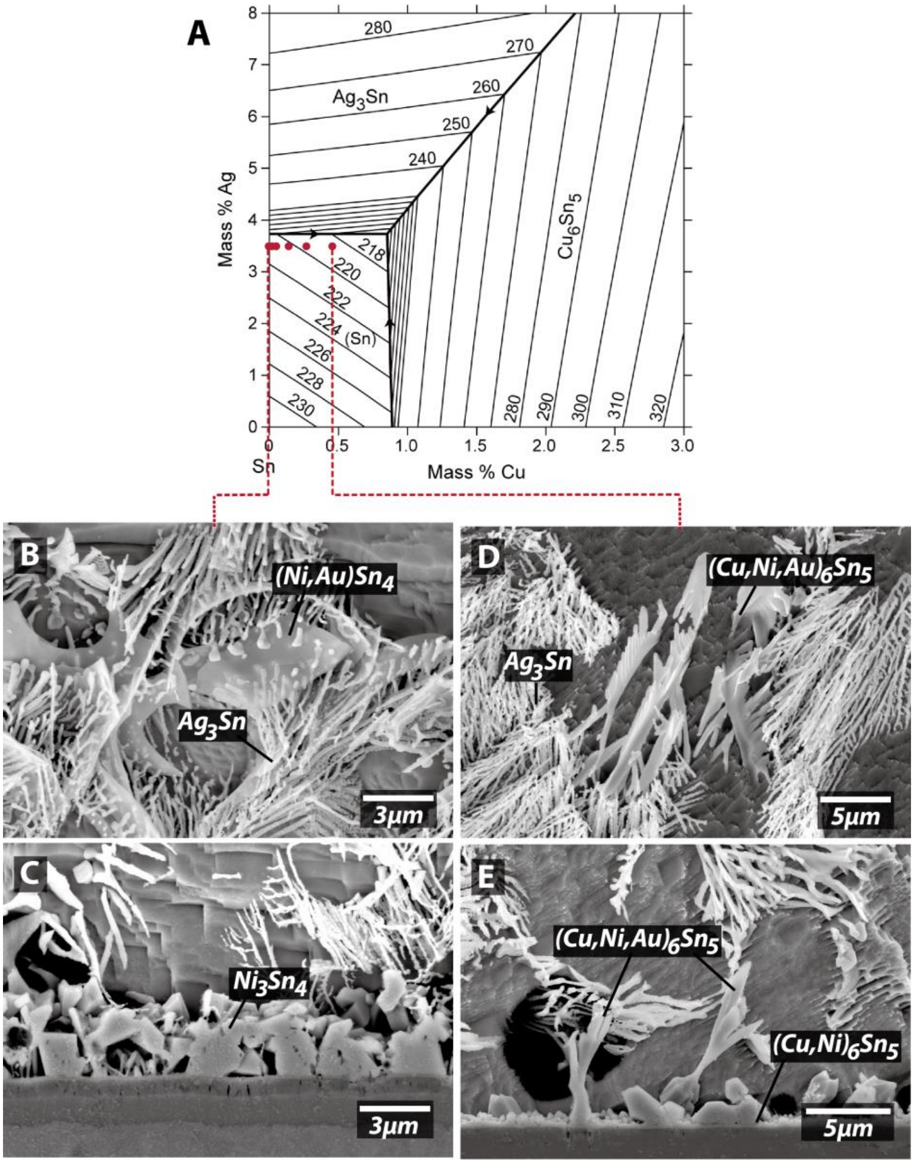

Figure 7. Sn-rich corner of Sn-Ag-Cu liquidus projection adopted from [39] with denoted Cu additions; representative eutectic microstructures and interfacial IMC layer formed in (B,C): Sn-3.5Ag/ENIG and (D,E): Sn-3.5Ag-0.5Cu/ENIG solder joints. Note that some βSn has been selectively etched.

Table 1. Summary of the SEM-EDX measurements for the eutectic $NiSn_4$ phase

Number of measurements		*Sn, at%*	*Ni, at%*	*Proposed phase*
21	Mean	81.4	18.6	**$NiSn_4$**
	St. dev.	0.67	0.67	

Table 2. Phases used for the assessment of the EBSPs collected from the Sn-Ni eutectic phase

Pearson Symbol	*Space Group (No.)*	*Phase/ Prototype*	*Mean MAD*	*a; b; c lattice parameters, Å*	*Ref.*
o*C*20	Aba2 (41)	$NiSn_4$	0.42	6.38; 6.42; 11.27	[24]
		$PdSn_4$	0.41	6.40; 6.43; 11.49	
		$PtSn_4$	0.41	6.40; 6.43; 11.38	
		$AuSn_4$	0.40	6.50; 6.54; 11.70	
t*P*10	P4/nbm (125)	$PtPb_4$	NI	6.67; 6.67; 5.98	[33]
t*I*40	I41/acd (142)	$\beta IrSn_4$	NI	6.31; 6.31; 22.77	[34]
m*C*14	C2/m (12)	Ni_3Sn_4	NI	12.21; 4.06; 5.22	[29]
o*P*20	Pnma (62)	Ni_3Sn_2	NI	4.15; 4.15; 5.25	[30]
h*P*8	P63/mmc (194)	Ni_3Sn	NI	5.19; 5.19; 4.14	[31]

NI = not indexable

Table 3. Summary of the SEM-EDX measurements for the eutectic phases formed in Sn-3.5Ag/ENIG and Sn-3.5Ag-0.005Cu/ENIG solder joints

	Sn, at%	*Ni, at%*	*Au, at%*	*Ag, at%*	*Cu, at%*	*Proposed phase*
			Sn-3.5Ag/ENIG solder joints			
Mean	81.6	12.4	6.0	-	-	**$(Ni,Au)Sn_4$**
St. dev.	0.72	0.72	1.11	-	-	
Mean	24.9	-	-	75.1	-	**Ag_3Sn**
St. dev.	0.54	-	-	0.54	-	
			Sn-3.5Ag-0.005Cu/ENIG solder joints			
Mean	81.1	12.7	6.2	-	-	**$(Ni,Au)Sn_4$**
St. dev.	0.94	0.94	1.34	-	-	
Mean	24.9	-	-	75.1	-	**Ag_3Sn**
St. dev.	0.54	-	-	0.54	-	
Mean	61.1	35.2	-	-	3.7	**$(Ni,Cu)_3Sn_4$**
St. dev.	2.48	2.64	-	-	0.71	
			At least 10 particles were measured for each phase			

Table 4. Intermetallic phases formed in Sn-3.5Ag-XCu (X = 0, 0.005, 0.01, 0.05, 0.15, 0.3 and 05wt%Cu) solders during soldering to Ni or ENIG plating

Sn-3.5Ag	***no Cu***	***0.005-0.01Cu***	***0.05Cu - 0.15Cu***	***0.3Cu***	***0.5Cu***
	2 IMCs:	***3 IMCs:***	***4 IMCs:***	***3 IMCs:***	***2 IMCs:***

bulk	Ag_3Sn **$(Ni,Au)Sn_4$**	Ag_3Sn **$(Ni,Au)Sn_4$** $(Ni,Cu)_3Sn_4$	Ag_3Sn **$(Ni,Au)Sn_4$** $(Ni,Cu)_3Sn_4$ $(Cu,Ni,Au)_6Sn_5$	Ag_3Sn $(Ni,Cu)_3Sn_4$ $(Cu,Ni,Au)_6Sn_5$	Ag_3Sn $(Cu,Ni,Au)_6Sn_5$
interface	Ni_3Sn_4	$(Ni,Cu)_3Sn_4$	$(Ni,Cu)_3Sn_4$	$(Ni,Cu)_3Sn_4$	$(Cu,Ni)_6Sn_5$